Particle Phase State and Aerosol Liquid Water Greatly Impact Secondary Aerosol Formation: Insights into Phase Transition and Role in Haze Events

Xiangxinyue Meng[1], Zhijun Wu[1,2*], Jingchuan Chen[1], Yanting Qiu[1], Taomou Zong[1], Mijung Song[3], Jiyi Lee[4], Min Hu[1,2]

1 State Key Joint Laboratory of Environmental Simulation and Pollution Control, International Joint Laboratory for Regional Pollution Control, College of Environmental Sciences and Engineering, Peking University, Beijing 100871, China

2 Collaborative Innovation Center of Atmospheric Environment and Equipment Technology, Nanjing University of Information Science and Technology, Nanjing 210044, China

3 Department of Earth and Environmental Sciences, Jeonbuk National University, Jeonju, Republic of Korea, 54896

4 Department of Environmental Science and Engineering, Ewha Womans University, Seoul, Republic of Korea, 03760

**Corresponding author: zhijunwu@pku.edu.cn*

Abstract. The particle-phase state is crucial for reactive gas uptake, heterogeneous, and multiphase chemical reactions, thereby impacting secondary aerosol formation. This study provides valuable insights into the significance of particle-phase transition and aerosol liquid water (ALW) in particle mass growth during winter. Our findings reveal that particles predominantly exist as semi-solid or solid during clean winter days with ambient relative humidity (RH) below 30%. However, non-liquid to liquid phase transition occurs when the ALW mass fraction exceeds 15% (dry mass) at transition RH thresholds of 40-60%. During haze episodes, the transformation rates of sulfate and nitrate aerosols rapidly increase through phase transition and increased ALW by 48% and 11%, respectively, resulting in noticeable increases in secondary inorganic aerosols (SIA). The presence of abundant ALW, favored by elevated RH and higher proportion of SIA, facilitates the partitioning of water-soluble compounds from gas to particle phase, as well as heterogeneous and aqueous processes in liquid particles. This leads to

a substantial increase in the formation of secondary organic aerosols and elevated aerosol oxidation. Consequently, the overall hygroscopicity parameters exhibit a substantial enhancement with a mean value of 23%. These results highlight phase transition as a key factor initiating the positive feedback loops between ALW and secondary aerosol formation during haze episodes over the North China Plain. Accurate predictions of secondary aerosol formation necessitate explicit consideration of the particle-phase state in chemical transport models.

1 Introduction

Submicron particles are ubiquitous in the nature, having great impacts on climate, visibility, and human health (Shiraiwa et al., 2011;Ravishankara, 1997;Pöschl, 2005;Lelieveld et al., 2015;Seinfeld et al., 2016;Hu et al., 2021). Phase state, a key parameter of particles, plays profound roles in the mass transport of reactive molecules between the gas phase and the particle phase (Marshall et al., 2018;Shiraiwa et al., 2011). This, in turn, influences the gas-particle partitioning of semi-volatile materials (Shiraiwa et al., 2013;Li and Shiraiwa, 2019), multiphase reaction rates of chemical species (Zhang et al., 2018;Mu et al., 2018), and even the ice nucleating activities of organic aerosols (OA) (Murray et al., 2010;Knopf and Alpert, 2023). Aerosol liquid water (ALW) contributes a substantial fraction of the mass in sub-micrometer particles on a global basis (Nguyen et al., 2016). Atmospheric particles with the presence of condensed water serve as suspended vessels of multiphase chemical reactions, leading to significant impacts on secondary aerosol formation, particle size growth, and air quality (Wu et al., 2018;Hodas et al., 2014;Liu et al., 2019). Therefore, a comprehensive understanding of particle-phase state and ALW is crucial for better evaluation of the related environmental effects.

In the real atmosphere, the particle-phase state varies significantly among solid, semi-solid, and liquid under different conditions, which specifically influenced by ambient relative humidity (RH), temperature, and aerosol chemical composition. For example, the atmospheric particles in the tropical rainforest over central Amazonia, which primarily consisted of secondary organic aerosols (SOA) derived from oxidation of isoprene, were observed to be in liquid state at RH > 80% (Bateman et al., 2016), but more non-liquid particles occurred with the impact of anthropogenic pollutants (Bateman et al., 2017). Liu et al. (2019) reported that particles with high mass fraction of inorganics and high RH were prone to be liquid in a subtropical coastal megacity. However, non-liquid particles appeared at RH < 60% in Beijing (Liu et al., 2017). Moisture can drive an RH-induced glass transition in particles, leading to a liquid state

and a significant water uptake at high RH in the lower atmosphere (Mikhailov et al., 2009). Moreover, organic aerosols might be in solid state at upper tropospheric temperatures that below about 210 K (Koop et al., 2011). Therefore, the changing features of aerosol composition and ambient RH may alter the ALW and trigger the phase state variation. More studies are needed to clarify the relationship between aerosol composition, particle-phase state, and ALW.

After the implementation of "China's Action Plan for Air Pollution Prevention and Control" in 2013, emissions of primary particulate matter and several gaseous pollutants have greatly reduced. However, the contribution and proportion of secondary inorganic aerosols (SIA) and secondary organic aerosols (SOA) have become increasingly significant (Lei et al., 2021;Wang et al., 2021b), especially during haze episodes in winter. As mentioned, particles changes from solid to liquid with elevated RH conditions during heavy haze episodes (Liu et al., 2017). In liquid particles, the gas-particle mass transfer for reactive gases can be greatly facilitated due to increased diffusion coefficients, and the thermodynamic equilibrium of semi-volatile compounds may be impacted to contribute to secondary aerosol formation (Shiraiwa et al., 2011;Jia et al., 2023). A recent field study by Gkatzelis et al. (2021) pointed out that the gas-to-particle partitioning in liquid particles enhances the uptake of water-soluble gas compounds, resulting in a 15-25% contribution of SOA mass during particulate pollution in Beijing. Many studies have demonstrated that the abundant ALW and high RH condition can greatly impact secondary aerosol formation processes (Xu et al., 2017;Wang et al., 2021a;Gkatzelis et al., 2021). However, there is still a lack of understanding regarding the role of phase state variations in secondary particulate pollution. In this study, we conducted a one-month field campaign in Beijing during winter to investigate the relationship between particle-phase state, ALW, and the chemical and physical processes involved in haze formation.

2 Methodology

2.1 Instruments and Measurements

Field campaigns were conducted in Beijing from 15th December 2020 to 10th January 2021 at the Changping campus of Peking University (40°8'N, 116°6'E). A detailed description of the sampling site can be found in previous studies (Wang et al., 2020c). The instruments were situated in the air monitoring laboratory, located on the top floor of the main building. A weather station (Met One Instruments Inc., USA), a suite of automatic gas analyzers (O_3, SO_2, CO and NO_x) from Thermo Scientific and an Aerodyne Quadrupole Aerosol Chemical Speciation Monitor (Q-ACSM) were operated according to standard protocols (Ng et al., 2011) and necessary information as described in Text S1.

The particle rebound fraction (f) was measured using a modified three-arm impactor (Bateman et al., 2014) coupled to a condensation particle counter (CPC, model 3772, TSI Inc.) with a time interval of 3 minutes, as described in our previous work (Liu et al., 2017;Meng et al., 2021). The three-arm impactor consisted of three parallel impactors with different designs. One of the impactors had no plate, while the others had plate equipped with an uncoated plate and a grease-coated plate, respectively. The no-plate impactor provided the total throughput rate, while the solid surface of the uncoated plate let particle rebound, and the sticky surface of the grease-coated plate captured all particles that struck it. To measure the f, a valve system with three solenoids and two actuators was used to ensure that the particle populations passing through the three impactors were sequenced and were measured by the CPC. Thus, rebound fraction, f, was defined as:

$$f = \frac{N_2 - N_3}{N_1 - N_3} \quad (1)$$

where N_1 was the whole particle population, N_2 was the population of particles that did not strike plus the rebounded particles from the impaction plate, and N_3 was the

population of particles that did not strike the impaction plate. Prior to measurement, we dried the particles to below 30% RH using a silica gel diffusion dryer. Then, 300 nm mono-disperse particles were selected by a Differential Mobility Analyzer (DMA, TSI model 3080). An RH adjustment system with two RH probes and a Nafion RH conditioner was employed to measure the RH conditions (ambient RH and impactor RH), as well as to adjust the impactor RH to match the real atmospheric RH. The measured impactor RH rapidly reached the ambient RH within 1 second, exhibiting a mean absolute error of 0.03. This swift regulation time is attributed to the real-time feedback in the RH control system, coupled with the typically modest fluctuations in ambient RH. Particles with a diameter of 300 nm, as selected for our study, rapidly achieved equilibrium in the humidification process, since the timescale for water diffusion into these particles is approximately 1 second, shorter than their residence time of about 3 seconds within the system. This is detailed in Text S2 and illustrated in Figure S1. Such conditions ensure that the measured particle rebound are representative and accurate at the ambient RH. Weekly calibrations using standard ammonium sulfate and daily flow check were conducted (Liu et al., 2021;Liu et al., 2019). Typically, $f <$ 0.2 or 0.1 are referred to the completely phase transition from non-liquid to liquid state (Pajunoja et al., 2016;Liu et al., 2017). In this study, we consider $f < 0.2$ in the case of liquid state. The time series of f with an initial time resolution is shown in Figure 1, while the data presented in other figures are all displayed as hourly averages.

2.2 Data Analysis

The mass concentrations of organics, sulfate, nitrate, ammonium, and chloride in non-refractory particles (NR-PM_1) were analyzed using the standard ACSM data analysis software (v.1.5.10). A collection efficiency (CE) of 0.5 was applied to the dataset (Xu et al., 2017;Matthew et al., 2008). Positive matrix factorization (PMF) was performed on the organic mass spectra using the Igor Pro based PMF2.exe algorithm to resolve primary organic aerosols (POA) and SOA factors. The data and error matrices were pretreated following methods from previous studies (Zhang et al., 2011;Zhang et al.,

2017). The key diagnostic plots are provided in supplementary (Figure S2-S3).

The aerosol liquid water content contributed by inorganics (ALW_{inorg}) in PM_1 was estimated using the ISORROPIA-II thermodynamic model (Fountoukis and Nenes, 2007) with input of aerosol chemical composition measured by Q-ACSM. The particles were assumed to be in metastable state, and the reverse mode was used to calculate the ALW_{inorg} due to absence of gaseous HNO_3 and NH_3. Besides, ALW associated with organics (ALW_{org}) was considered using a simplified equation of *k*-Köhler theory (Guo et al., 2015;Petters and Kreidenweis, 2007):

$$ALW_{org} = V_{org} k_{org} \frac{a_w}{1-a_w}, \quad (2)$$

where V_{org} is the volume concentration of organics with a typical density of 1.4 g/cm^3 (Cerully et al., 2015), k_{org} is the hygroscopicity parameter of the organics, a_w represents the water activity, which is assumed to have the same value as RH. In this study, we used a fixed k_{org} of 0.06 to evaluate ALW_{org}, which was the average value of the overall k_{org} in the consideration of POA and SOA contributions in the total non-refractory organics (k_{POA} = 0 and k_{SOA} = 0.1) (Wu et al., 2016;Gunthe et al., 2011). However, it should be noted that k_{org} has been found to exhibit a positive linear relationship with the aerosol oxidation degree, which varied among species (Chang et al., 2010;Duplissy et al., 2011). f_{44}, the fraction of m/z 44 fragment signal to total organic signal, is widely used to represent the atmospheric aging process of OA species (Ng et al., 2010;Canagaratna et al., 2015). Real-time k_{org} was $k_{org} = 1.04 \times f_{44} - 0.02$, as reported by Kuang et al. (2020) for the North China Plain (NCP). The predicted real-time k_{org} ranged from 0.13 to 0.24, which was consistent with the variation range reported for winter Beijing (0.06-0.3) (Li et al., 2019;Jin et al., 2020). For fixed k_{org}, the contribution of organics to ALW was ~12% on average during the observation. However, considering the variation of real-time f_{44}, organics were capable to provide more than 30% and 20% of the total ALW mass on average during clean and polluted days, respectively (Figure S4 and Text S3). In recognition of ALW's plasticizing effect

on particle-phase state, the potential impacts of whether the hygroscopicity value of organics is fixed or varies in real-time on phase transition has been discussed in Section 3.2.

For a given internal mixture, the overall particle hygroscopicity (k_{total}) was calculated by a simple mixing rule by weighting the hygroscopicity parameters of the components by their volume fractions in the mixture (Petters and Kreidenweis, 2007):

$$k_{total} = k_{inorg} \cdot frac_{inorg} + k_{org} \cdot frac_{org}, \quad (3)$$

Where $frac_{inorg}$ and $frac_{org}$ are the inorganics and organics volume fractions in NR-PM_1, respectively. Considering the variability in the composition of inorganics and organics, the hygroscopicity parameters of inorganics (k_{inorg}) was weighted by volume fractions. The main form of inorganic species (NH_4NO_3 and $(NH_4)_2SO_4$) in the urban atmosphere was considered due to the lower abundance of chloride in NR-PM_1. The volume fraction of each inorganic species was calculated based on the ion-pairing scheme as described in Gysel et al. (2007) with their gravimetric density (1720 kg m^{-3} for NH_4NO_3 and 1769 kg m^{-3} for $(NH_4)_2SO_4$) (Wu et al., 2016). The hygroscopicity parameters of NH_4NO_3 and $(NH_4)_2SO_4$ are 0.58 and 0.48, respectively following previous studies (Wu et al., 2016;Jin et al., 2020;Petters and Kreidenweis, 2007). For hygroscopicity parameters of organics (k_{org}), real-time k_{org} were used as above, which effectively captured the characteristics of the investigated area in our study.

3 Results and Discussion

3.1 Chemical Composition and Phase State of Sub-micrometer Particles

Figure 1 shows the time series of meteorological parameters, chemical composition of NR-PM_1, gas pollutants, and particle rebound fraction from December 16, 2020, to January 10, 2021. The average mass concentration of NR-PM_1 was 15.8±16.8 μg m^{-3} during the measurement period. During clean periods (NR-PM_1 < 20 μg m^{-3}), organics dominated the aerosol composition, accounting for ~45% of NR-PM_1 mass. Nitrate,

sulfate, and ammonium contributed 20%, 16%, and 16% to total NR-PM_1 on average, respectively (Figure S5). However, several pollution episodes occurred with rapid growth in NR-PM_1 and ALW mass concentration with higher concentrations of NO_x and SO_2, as marked by yellow shadow in Figure 1. These four polluted episodes typically started with ambient RH below 40% and higher O_3 levels (> 30 ppb) and mounted up with stagnant meteorological conditions bringing high RH (> 60% RH) and low surface wind speed (< 3 m/s). This meteorological pattern is commonly observed over the NCP during haze episodes (Sun et al., 2013;Sun et al., 2015). During these polluted episodes, nitrate increased rapidly accounting for an average of 33% of the total NR-PM_1 mass. ALW was minor during clean days, but increased up to 26% in PM_1 during severe polluted episodes with NR-PM_1 > 80 μg m^{-3} (Figure S6). The mass concentrations of POA and SOA both increased during these polluted episodes as shown in Figure 1d. Moreover, the mass contribution of SOA to total OA showed an upward trend in particulate mass, indicating the important contribution of secondary formation during haze formation (Figure S7).

As shown in Figure 1f, particle rebound fraction, *f*, varied with ambient RH from 1.0 to ~0.0 during the observation, indicating that particles possessed phase transition from non-liquid to liquid state. Similar patterns of particle-phase transition were found for several polluted episodes. Taking P4 as an example, *f* remained stable at 0.8 with RH = ~20% during the initial period of stagnant conditions, but gradually dropped to ~0.1 along with the increasing RH and NR-PM_1 during the subsequent haze formation. In addition, we collected several $PM_{2.5}$ filter samples to characterize the bulk-phase viscosity during clean and polluted days based on poke-and-flow experiment, as described in our previous study (Song et al., 2022) and Text S4 (indicated by black and red frames in Figure 1f). As shown in Figure S8, the viscosity was proved to be higher than ~10^8 Pa s with a mean value of *f* > 0.8 during clean days, indicating that particles existed in a solid or semi-solid state. However, the viscosity was lower than ~10^2 Pa s with an average *f* <0.2 under higher RH conditions during polluted days, indicating the

liquid state. It should be noted that the viscosity measurement captured the bulk-phase viscosity for water soluble components in $PM_{2.5}$ filter samples, but the online measurement of *f* depicted 300 nm particles representative of accumulation mode particles, which normally contributed the majority fraction of PM_1. While the differences in chemical composition between $PM_{2.5}$ filter samples and 300 nm particles may introduce uncertainties when comparing the phase state of the targeted aerosols, the viscosity results showed good agreement with the average variation of *f* during the corresponding period. Further validation is still necessary to compare the two different techniques and will be displayed in our further study. To directly indicate the phase transition from the perspective of viscosity, RH-dependent *f* was measured for these filter samples with known bulk-phase viscosity (Figure S9 and Text S5). As expected, the decreasing *f* from >0.8 to 0 covered the transition range from ~10^8 Pa s to ~10^2 Pa s, which indicated the consistent behavior of particle rebound and measured bulk-phase viscosity for the investigated aerosols.

3.2 Phase Transition Behavior of Sub-micrometer Particles

Figure 2a illustrates the frequency distribution of RH. *f* as a function of RH were plotted in Figure 2b. During the observation, ambient RH was below 30% for more than half of the time with *f* predominantly exceeding 0.8 under such conditions. When RH increased to ~50-60%, a majority of *f* dropped to <0.2 along with the increasing NR-PM_1 mass. This means that particles went through a moisture-induced phase transition from non-liquid to liquid during haze formation when RH reached 60%, which aligned with our previous studies (Liu et al., 2017). Notably, some points with higher mass fraction of inorganics (f_{inorg} > 0.7) showed $f < 0.2$ at RH = 40-50%, indicating that particles with higher f_{inorg} were already in a liquid state. Consequently, particles underwent phase transition with a relatively large RH range of 40-60%, exhibiting varying chemical compositions as marked by the red frame.

Particle-phase state is known to be sensitive to ALW by its unique plasticizer effect

(Koop et al., 2011). In Figure 2d, f as a function of ALW/NR-PM_1 were plotted to represent the relative water uptake of unit mass dry aerosols with corresponding particle rebound behaviors. Figure 2c displays the frequency distribution of three f intervals in each ALW/NR-PM_1 bin. When ALW/NR-PM_1 < 5%, the frequency of f > 0.8 was higher than 0.65, indicating that particles mostly stay in a more viscous non-liquid state with less water uptake capacity. When ALW/NR-PM_1 increased to 5-15%, f gradually decreased from 0.8 to 0.2, suggesting that the total water uptake gradually enhanced and lowered the viscosity to trigger the phase transition within this range. The non-liquid particles were dominant with the frequency of f=0.2-0.8 close to 0.8. When ALW/NR-PM_1 > 15%, the frequency of f < 0.2 dramatically increased from 0.2 to ~0.8, reaching close to 1.0 at ALW/NR-PM_1 > 25% with higher particulate mass. This indicates that particles mostly convert to liquid when the mass fraction of ALW surpasses a certain threshold during haze formation, rather than the absolute ALW mass (Figure S10). In general, a good correlation between ALW/NR-PM_1 and f was observed. ALW/NR-PM_1, used as a mass-based hygroscopic growth factor (Chen et al., 2022;Liu et al., 2018), is suitable to quantify the moisture-induced phase transition capacity of atmospheric particles, and a value of 15% can be the sudden change in the case of phase transition from non-liquid to liquid.

It should be noted that calculations of ALW in this study have considered inorganic salts and organics. Acknowledging that the hygroscopicity of organics, characterized by either a fixed k_{org} or varying in real-time, affects the calculation of ALW mass, a sensitivity analysis examining its impact on the phase transition threshold (ALW/NR-PM_1) is presented in Figure S11. There is no denying that the contribution of inorganic salts to ALW remains predominant, with their contribution to ALW being ~88% (a fixed k_{org} of 0.06) and ~73.5% (real-time k_{org}) on average during the observation (Figure S4), indicating that the impact of different ALW calculations on ALW/NR-PM_1 values was minor. As expected, the frequency distribution of these three f intervals showed no obvious change for ALW calculations by inorganics, fixed k_{org}, and real-time k_{org} at the

whole ALW/NR-PM_1 range. Although the frequency of $f < 0.2$ changed from ~0.8 to 0.5 at ALW/NR-PM_1 = 15-20% when shifting to real-time k_{org}, the frequency remained higher than 0.5 and approached 1.0 with larger ALW/NR-PM_1 values. This indicates that while the varying k_{org} impacts the number of data points within ALW/NR-PM_1 bins of 15-20%, it does not affect the overall transition trend. As a result, the impacts of different ALW calculation on ALW/NR-PM_1 were not significant, and the phase transition threshold of 15% remains valid. It is suggested that caution should be exercised when using the above approach to characterize the phase state of targeted aerosols, as the measured f was representative of accumulation mode particles that dominated the mass concentration of submicron particles (Seinfeld, 2006).

It is interesting to note that several points with ALW/NR-PM_1 < 5% and NR-PM_1 >30 μg/m^3 exhibited lower rebound fraction ($f < 0.4$), which was attributed to the variation of RH background from high RH to low RH during the later stages of the haze episodes, as shown in Figure 2d and Figure S12. This suggests that liquid particles may not turn to be a more viscous semi-solid state in a brief period under dehydration process. There are two possible explanations for this phenomenon. Firstly, the presence of significant amounts of inorganic and organic compounds can alter the humidity conditions for deliquescence and efflorescence (Ushijima et al., 2021;Peckhaus et al., 2012). Secondly, these particles are likely become non-ideal mixing due to drying process that form core-shell structure (Shiraiwa et al., 2013;Ciobanu et al., 2009;Song et al., 2013). Studies have revealed that outer phase may form viscous organic shell to prevent water evaporation (Koop et al., 2011;Shiraiwa et al., 2013;Hodas et al., 2015), thus, the inner phase containing inorganics still keep liquid with residual water. However, it should be noted that liquid-liquid phase separation was not optically detected under staged dehydration of filter-based Beijing $PM_{2.5}$ droplets by Song et al. (2022). Instead, they observed abrupt effloresced inorganics at ~30% RH, which was much lower than $(NH_4)_2SO_4$ and NH_4NO_3 in pure form (Peng et al., 2022). This supports that atmospheric particles are more likely to be metastable after liquification only if RH

decreases to very low values.

In addition to RH and aerosol compositions, environmental temperature also plays a significant role in determining the phase state (Koop et al., 2011;Shiraiwa et al., 2017;Petters et al., 2019). A reduction in temperature results in higher viscosity, whereas a rise in RH leads to a decrease in viscosity, attributed to the plasticizing effect of water (Koop et al., 2011). Although the relationship between *f* and temperature is not strongly evident as that of RH in this study (Figure S13), it's observed that a greater number of data points exhibited near 0.9 under low RH conditions (<30%), suggesting higher viscosity at colder temperatures (< -10 ℃) than warmer scenarios. The glass transition temperature (T_g) is a key metric for the non-equilibrium phase transition from a glassy solid to a semi-solid state as temperature rises (Koop et al., 2011). Particles act as solid when the temperature falls below T_g ($T_g/T>1$), and transition to semi-solid or liquid at temperature exceeding T_g. An increase in compound molecular weight, O:C ratio, and functional group composition are identified as key factors affecting the T_g of OA (Saukko et al., 2012;Dette et al., 2014;Rothfuss and Petters, 2017;Shiraiwa et al., 2017). Shiraiwa et al (2017) proposed that T_g/T is an indicator for the semi-solid to liquid phase transition of OA, with a threshold of $T_g/T\approx0.8$. In this study, we employed a T_g parameterization method for OA viscosity based on their molecular weight and O:C ratio to assess the combined effects of aerosol composition, RH and temperature on particle phase state (Shiraiwa et al., 2017). This method accounts for water associated with both inorganics and organics, rather than focusing solely on organics, to calculate T_g of ambient OA, as elaborated in Text S6.

Figure 3a displays the characteristic relations between T_g/T and ALW/NR-PM_1 with different approach for T_g calculations of ambient OA. Different phase state intervals are characterized by T_g/T based on predicted viscosity η as shown in Figure 3b, and are illustrated using dashed lines with arrows. The predicted viscosity η of OA was calculated by applying the Vogel–Tammann–Fulcher (VTF) equation (Angell, 1991) with a fragility parameter of 10 (DeRieux et al., 2018). Clearly, after calculating T_g in

conjunction with k_{total}, there is a strong consistency in the characteristic relationship between the estimated T_g/T and ALW/NR-PM_1 with both fixed and variable k_{org}. This consistency aligns well with the phase state changes of atmospheric aerosols discussed earlier in this study. In contrast, even when accounting for variations in hygroscopicity due to different oxidation degrees of OA, the majority of these estimated T_g/T values fall within the semi-solid and solid range at higher ALW/NR-PM_1, significantly deviating from the field observations. This highlights the significant impact of environmental RH and chemical composition on the moisture-induced phase transition of atmospheric particles in the near-surface atmosphere. In particular, inorganic salts play a dominant role, contributing more significantly to the mass fraction of ALW in total particulate matter. The estimated T_g/T for ambient OA with k_{total} transitioned to a liquid state at ALW/NR-PM_1 > 10%, which is slightly lower than the transition threshold of 15% proposed in this study. It should be noted that the estimated T_g of OA adopted an average molecular weight (MW) of 200 g mol^{-1}, as used in previous studies (Williams et al., 2010;Shen et al., 2018). However, the average MW of ambient OA is likely variable due to the atmospheric aging process. Increasing the value of MW can shift the characteristic cure of T_g/T versus ALW/NR-PM_1 to the right, thereby aligning the semi-solid to liquid transition threshold more closely with the results observed in this study. This further suggests that incorporating of k_{total} into T_g calculation may potentially enhance the simulation results, especially in regions with a high proportion of inorganic salts under humid conditions. It should be noted that this aspect warrants further exploration in subsequent research.

3.3 Effects of Phase Transition and ALW on SIA Formation during Haze Episodes

We investigated the *f* and secondary aerosols during four polluted episodes (P1 to P4) under stagnant weather conditions with WS < 3 ms^{-1}. Sulfur and nitrogen oxidation ratios, SOR ($nSO_4/(nSO_4 + nSO_2)$) and NOR ($nNO_3/(nNO_3 + nNO_2)$), commonly used as indicators for secondary inorganic transformation (Li et al., 2017), are plotted as a function of *f* in Figure 4a and 4b. We found that SOR (NOR) remained in a lower

level with a mean value of ~0.27 (0.08) at f > 0.2 for non-liquid particles, but increased significantly to ~0.8 (0.35) with increasing ALW/NR-PM_1 at f < 0.2. This indicates that the secondary formation of SIA is facilitated to a certain degree through phase transition and the increasingly higher ALW mass. It should be noted that particles can be non-liquid during haze episodes with f =1.0-0.2. Interestingly, SOR and NOR remained in lower levels and did not show notable increase between f = 1.0-0.8 and f = 0.8-0.2, until particles accomplished the phase transition at f = 0.2-0.0 (Figure 4c1 and 4c2). As a result, the median SOR (NOR) increased to higher levels with an increment of 48% (11%) via phase transition along with the increase in ALW.

From the perspective of phase state, the increasing mass fraction of ALW reduces the viscosity and triggers the phase transition, which have important roles in the gas-particle mass transfer during haze formation. It is suggested that the secondary transformation of SIA is impeded by limited mass transfer between gas and particle phase when particles are not fully converted into liquid state. However, these limited factors disappear or the dominant formation pathway changes after phase transition. As reported in previous studies, ALW facilitates the secondary formation of sulfate and nitrate via the promotion of heterogeneous reactions (e.g. SO_2 heterogeneous oxidation, N_2O_5 hydrolysis), gas-particle partitioning of semi-volatile components or aqueous-phase reactions on wet aerosols (Chen et al., 2022;Cheng et al., 2016;Wang et al., 2020b;Liu et al., 2020). However, aqueous-phase oxidation of SO_2 may be constrained before phase transition due to the low diffusivity of multiple oxidants (e.g. O_3, H_2O_2 and NO_2) in the particles, and it may become the dominant formation pathway in liquid particles (Ravishankara, 1997;Liu et al., 2020). Additionally, the partitioning of nitrate into particles following Henry's Law may also be facilitated by the increased ALW due to enhanced diffusivity of dissolved precursors in liquid particles. In Figure 4d, the mass fraction of SIA ($f_{SIA/NR\text{-}PM_1}$) is plotted as a function of f. The $f_{SIA/NR\text{-}PM_1}$, ALW mass concentration, and RH were grouped and averaged corresponding to f bin width of 10%. We found that $f_{SIA/NR\text{-}PM_1}$ remained stable at f = 1.0-0.4, but steadily increased from an

average of ~0.50 to ~0.65 with elevated RH levels (>40%) and decreasing *f* (from 0.4 to 0.0). This indicates that SIA formation was limited for non-liquid particles with higher viscosity under lower RH conditions. However, ALW was steadily enhanced by the increasing RH and started to trigger the phase transition, thereby facilitating the SOR and NOR to a larger extent. Therefore, $f_{SIA/NR\text{-}PM_1}$ apparently increased with the increase in ALW at *f* = 0.2-0.0. The presence of more ALW in liquid particles was expected to promote the SIA formation by acting as multiphase reaction vessels (Zheng et al., 2015;Wang et al., 2020a;Wang et al., 2020b). One should note that, the average environmental temperature during pollution episodes increased to approximately 0°C, in contrast to the -10°C recorded during clean periods. The rise in ambient temperature typically enhances the diffusivity of atmospheric reactive molecules in both the gas and particle phases (Tang et al., 2014;Shiraiwa et al., 2011;Li and Shiraiwa, 2019). This, in turn, may potentially influence the heterogeneous or liquid-phase reactions, and even the gas-particle partitioning of semi-volatile compounds.

3.4 Effects of Phase Transition and ALW on SOA Formation during Haze Episodes

In Figure 5a and 5b, the ratio of SOA to POA (SOA/POA) is plotted as a function of *f* during these four polluted episodes characterized by ALW/NR-PM_1 and f_{44}. For *f* = 1.0-0.2, particles possessed relatively lower SOA/POA values (1-2.5) with ALW/NR-PM_1 <15%, which was independent of NR-PM_1 mass concentrations. However, a noticeable increase in SOA/POA and elevated f_{44} values were observed at *f* = 0.2-0.0, accompanied by increasing ALW/NR-PM_1 and NR-PM_1 mass. This indicates that more oxidized SOA was produced in liquid particles through the phase transition and the increasing mass fraction of ALW during haze formation. Interestingly, we observed that these liquid particles were primarily associated with polluted days during the nighttime (Figure S14). For these liquid particles, SOA/POA doubled to ~5.5 along with the increasing f_{44} compared to non-liquid particles, suggesting the important roles of phase transition and ALW in promoting the SOA formation through dark reactions during nighttime. From the perspective of phase state, phase transition was directly indicated by the

decreasing *f* during haze formation driving a large decrease in bulk phase viscosity from $>10^8$ Pa s to $<10^2$ Pa s as proved by viscosity measurement, which may enhance the gas-particle mass transfer. ALW reduces the viscosity and triggers the phase transition, thus facilitating the uptake of precursors and oxidants, and potentially altering the reaction pathway (Tillmann et al., 2010;Berkemeier et al., 2016;Li et al., 2018;Zhao et al., 2019).

For non-liquid particles, ALW facilitates the SOA formation via partition and heterogeneous uptake of water-soluble organics from gas phase into the particle phase, leading to a rapid increase in SOA along with ALW (Herrmann et al., 2015;Gkatzelis et al., 2021;Lim et al., 2010;El-Sayed et al., 2015). Subsequent aqueous-phase reactions may occur to form oligomers, organosulfates, and nitrogen-containing organics through radical or non-radical reactions (Surratt et al., 2007;Iinuma et al., 2007;Galloway et al., 2009;Lim et al., 2013;Wang et al., 2020c). However, these reactions may be limited in non-liquid particles by the lower diffusivity due to higher viscosity. In contrast, liquid particles provide unstrained mass transfer of necessary oxidants and precursors between gas and particle phase, which is favorable for aqueous-phase processing. It is well known that aqueous-phase processing can contribute more oxidized SOA (Xu et al., 2017;Ervens et al., 2011;Zheng et al., 2023). Recent field studies have demonstrated that oligomers or dicarboxylic acids were enriched in liquid particles from the reactive uptake of methylglyoxal during the severe haze episodes in Beijing (Zheng et al., 2021). These oxidation products formed through aqueous-phase reactions are typically more oxidized and less volatile than those formed through gas phase photochemistry (Ervens et al., 2011), which can be reserved in the particle phase and increased the SOA mass in total OA. Therefore, the significant growth of SOA/POA and f_{44} after phase transition is attributed by the enhanced heterogeneous or aqueous-phase reactions in liquid particles with abundant ALW during the nighttime.

3.5 Positive Feedback Loops between ALW and Secondary Aerosol Formation Triggered by Phase Transition during Haze Episodes

In Figure 6a, the relationship between the overall particle hygroscopicity(k_{total}) and RH is displayed. The k_{total}, ALW, and NR-PM_1 mass were grouped and averaged corresponding to an RH bin width of 10%. When RH was below 30%, the averaged k_{total} was ~0.35. However, it increased to 0.39 with higher ALW and NR-PM_1 mass at RH =40-60%, and further rose to 0.43 with an average maximum NR-PM_1 value of 56 μg/m^3 when RH reached 70-80%. This indicates that hygroscopic growth of particulate matter underwent two stages with increasing RH and NR-PM_1 mass, particularly at RH = 40-60% and RH > 70%. From the above discussion, we have demonstrated that the non-liquid to liquid phase transition was triggered by the increased ALW, with a transition RH threshold of 40-60% during haze episodes (as indicated by gradual color change in Figure 6a). Phase transition facilitated the formation of sulfate and nitrate aerosols, contributing higher proportion of SIA in total particles under higher RH conditions. Notably, this led to a continuous increase in the volume fraction of inorganics with increasing RH (Figure 6b). Besides, k_{inorg} also slightly increased when RH reached 60% due to increased nitrate contribution in total SIA during haze episodes (Figure 6c and Figure S5). This may explain the first enhancement of k_{total} at RH = 40-60%, which was mainly driven by the large increase in $frac_{inorg}$ favored by phase transition.

Furthermore, the increase in k_{total}, coupled with elevated RH levels, led to a greater abundance of ALW mass. Heterogeneous or aqueous-phase reactions were favored with increasing ALW, promoting the formation of more oxidized SOA in liquid particles. At RH > 70%, the significant increase in k_{org} (~14%) compensated for the negative effect of decreased $frac_{org}$ on the total hygroscopicity contributed by organics (k_{org}·$frac_{org}$), leading to a stable k_{org}·$frac_{org}$ with increasing RH (Figure 6c and Figure S15). This, in turn, coordinated with the increased $frac_{inorg}$, resulting in the second enhancement of

k_{total}. As a result, phase transition accompanied by increasing ALW mass triggered a noticeable enhancement in k_{total} with a mean value of 23% during haze episodes. The enhanced water uptake ability of aerosols is expected to contribute more ALW under elevated RH conditions, further facilitating the secondary aerosol formation and deteriorating air quality. These results indicate that the establishment of positive feedback loops between ALW and secondary aerosol formation was triggered by phase transition during haze episodes.

4 Conclusion and atmospheric implications

Our findings revealed that particles predominantly exist as semi-solid or solid during clean winter days with RH below 30%. However, non-liquid to liquid phase transition occurred when the ALW mass fraction surpassed 15% (dry mass) at transition RH thresholds ranging from 40% to 60%. Additionally, we observed a consistent pattern in the non-liquid to liquid phase transition during haze formation, as manifested by both particle-rebound fraction and bulk-phase viscosity measurements. Specifically, the decrease in f from >0.8 to 0 corresponded to a viscosity transition ranging from ~10^8 Pa s to ~10^2 Pa s. With the incorporation of k_{total} into T_g calculation for ambient OA, we found that the characteristic of T_g/T versus ALW/NR-PM_1 agrees well with our field observations. This finding offers insights into the effectiveness of ALW/NR-PM_1 as an indicator for quantifying the moisture-induced phase transition capacity of atmospheric particles. Furthermore, incorporating overall particle hygroscopicity into the T_g calculation may potentially enhance OA viscosity simulations, especially in regions with a high proportion of inorganic salts under humid conditions. During haze episodes, SOR and NOR rapidly increased through phase transition and increased ALW by 48% and 11%, respectively, resulting in noticeable increases in SIA. The presence of abundant ALW, favored by elevated RH and higher proportion of SIA, facilitates heterogeneous and aqueous processes in liquid particles, leading to a substantial increase in the formation of secondary organic aerosols and elevated aerosol oxidation. As a result, the overall hygroscopicity parameters exhibit a substantial enhancement

with a mean value of 23%.

In our previous studies, we have revealed the positive feedback loops between ALW and anthropogenic SIA at elevated RH levels during haze formation (Wu et al., 2018;Wang et al., 2020b). The contribution of abundant ALW to SOA production has also been reported in various regions with active anthropogenic emissions, such as the Po Valley in Italy, southeastern U.S., and Beijing, China (Carlton and Turpin, 2013;Hodas et al., 2014;Xu et al., 2017). However, we observed that secondary transformation of SIA and SOA was significantly enhanced after phase transition with higher ALW mass during the observation. Our findings indicate that the secondary aerosol formation could be impeded on non-liquid particles due to limited mass transfer between gas and particle phase for relevant reaction components (Ravishankara, 1997;Shiraiwa et al., 2011;Abbatt et al., 2012;Ma et al., 2022), whereas it is facilitated in liquid particles. It is therefore recommended that non-liquid to liquid phase transition may be considered to be the kick-off for the positive feedback loops between ALW and secondary aerosol formation during haze events. This can be further supported by the case studies for varying polluted episodes, where episodes with phase transition generally exhibit higher secondary transformation rate of secondary aerosols compared to episodes without phase transition (Figure S16 and Text S7). This mechanism is expected to gain significance in other regions with abundant anthropogenic emissions and high background RH during haze formation.

Author contributions

X.X.Y.M. and Z.J.W. conceived the study. X.X.Y.M. conducted the experiments, analyzed the experimental data, and wrote the manuscript with contributions from Z.J.W., M.J.S., J.Y.L. and M.H. J.C.C. participated in the offline experiments and data analysis. Y.T.Q. and T.M.Z. participated in the field experiments and conducted the filter sampling.

Funding

This work was supported by the National Natural Science Foundation of China (Grant No. 42375093) and the Fine Particle Research Initiative in East Asia Considering National Differences (FRIEND) Project through the National Research Foundation of Korea (NRF: 2020M3G1A1114537) funded by the Ministry of Science and ICT, Korea.

Data availability

The data presented in this article can be accessed through the corresponding author Zhijun Wu (zhijunwu@pku.edu.cn).

Acknowledgments

We sincerely thank our two referees for their valuable comments and constructive suggestions to improve the scientific and rigorous nature of our manuscript. We gratefully acknowledge the assistance of Wenfei Zhu for the technical support on Q-ACSM running and instrument calibration during the campaign.

Competing interests

The authors declare that they have no conflict of interest.

Reference

Abbatt, J. P. D., Lee, A. K. Y., and Thornton, J. A.: Quantifying trace gas uptake to tropospheric aerosol: recent advances and remaining challenges, Chem. Soc. Rev, 41, 6555-6581, 2012.

Angell, C. A.: Relaxation in Liquids, Polymers and Plastic Crystals - Strong Fragile Patterns and Problems, J Non-Cryst Solids, 131, 13-31, 1991.

Bateman, A. P., Belassein, H., and Martin, S. T.: Impactor Apparatus for the Study of Particle Rebound: Relative Humidity and Capillary Forces, Aerosol Sci. Technol., 48, 42-52, 10.1080/02786826.2013.853866, 2014.

Bateman, A. P., Gong, Z. H., Liu, P. F., Sato, B., Cirino, G., Zhang, Y., Artaxo, P., Bertram, A. K., Manzi, A. O., Rizzo, L. V., Souza, R. A. F., Zaveri, R. A., and Martin, S. T.: Sub-micrometre particulate matter is primarily in liquid form over Amazon rainforest, Nat. Geosci., 9, 34-+, 2016.

Bateman, A. P., Gong, Z. H., Harder, T. H., de Sa, S. S., Wang, B. B., Castillo, P., China, S., Liu, Y. J., O'Brien, R. E., Palm, B. B., Shiu, H. W., Cirino, G. G., Thalman, R., Adachi, K., Alexander, M. L., Artaxo, P., Bertram, A. K., Buseck, P. R., Gilles, M. K., Jimenez, J. L., Laskin, A., Manzi, A. O., Sedlacek, A., Souza, R. A. F., Wang, J., Zaveri, R., and Martin, S. T.: Anthropogenic influences on the physical state of submicron particulate matter over a tropical forest, Atmos. Chem. Phys., 17, 1759-1773, 2017.

Berkemeier, T., Steimer, S. S., Krieger, U. K., Peter, T., Pöschl, U., Ammann, M., and Shiraiwa, M.:

Ozone uptake on glassy, semi-solid and liquid organic matter and the role of reactive oxygen intermediates in atmospheric aerosol chemistry, Phys. Chem. Chem. Phys., 18, 12662-12674, 10.1039/C6CP00634E, 2016.

Canagaratna, M. R., Jimenez, J. L., Kroll, J. H., Chen, Q., Kessler, S. H., Massoli, P., Hildebrandt Ruiz, L., Fortner, E., Williams, L. R., Wilson, K. R., Surratt, J. D., Donahue, N. M., Jayne, J. T., and Worsnop, D. R.: Elemental ratio measurements of organic compounds using aerosol mass spectrometry: characterization, improved calibration, and implications, Atmos. Chem. Phys., 15, 253-272, 10.5194/acp-15-253-2015, 2015.

Carlton, A. G., and Turpin, B. J.: Particle partitioning potential of organic compounds is highest in the Eastern US and driven by anthropogenic water, Atmos. Chem. Phys., 13, 10203-10214, 10.5194/acp-13-10203-2013, 2013.

Cerully, K. M., Bougiatioti, A., Hite Jr, J. R., Guo, H., Xu, L., Ng, N. L., Weber, R., and Nenes, A.: On the link between hygroscopicity, volatility, and oxidation state of ambient and water-soluble aerosols in the southeastern United States, Atmos. Chem. Phys., 15, 8679-8694, 10.5194/acp-15-8679-2015, 2015.

Chang, R. Y. W., Slowik, J. G., Shantz, N. C., Vlasenko, A., Liggio, J., Sjostedt, S. J., Leaitch, W. R., and Abbatt, J. P. D.: The hygroscopicity parameter (κ) of ambient organic aerosol at a field site subject to biogenic and anthropogenic influences: relationship to degree of aerosol oxidation, Atmos. Chem. Phys., 10, 5047-5064, 10.5194/acp-10-5047-2010, 2010.

Chen, Y., Wang, Y., Nenes, A., Wild, O., Song, S. J., Hu, D. W., Liu, D. T., He, J. J., Ruiz, L. H., Apte, J. S., Gunthe, S. S., and Liu, P. F.: Ammonium Chloride Associated Aerosol Liquid Water Enhances Haze in Delhi, India br, Environ. Sci. Technol., 56, 7163-7173, 10.1021/acs.est.2c00650, 2022.

Cheng, Y., Zheng, G., Wei, C., Mu, Q., Zheng, B., Wang, Z., Gao, M., Zhang, Q., He, K., Carmichael, G., Pöschl, U., and Su, H.: Reactive nitrogen chemistry in aerosol water as a source of sulfate during haze events in China, Sci. Adv., 2, e1601530, doi:10.1126/sciadv.1601530, 2016.

Ciobanu, V. G., Marcolli, C., Krieger, U. K., Weers, U., and Peter, T.: Liquid-Liquid Phase Separation in Mixed Organic/Inorganic Aerosol Particles, J. Phys. Chem. A, 113, 10966-10978, 2009.

DeRieux, W. S., Li, Y., Lin, P., Laskin, J., Laskin, A., Bertram, A. K., Nizkorodov, S. A., and Shiraiwa, M.: Predicting the glass transition temperature and viscosity of secondary organic material using molecular composition, Atmos Chem Phys, 18, 6331-6351, 2018.

Dette, H. P., Qi, M., Schröder, D. C., Godt, A., and Koop, T.: Glass-Forming Properties of 3-Methylbutane-1,2,3-tricarboxylic Acid and Its Mixtures with Water and Pinonic Acid, The Journal of Physical Chemistry A, 118, 7024-7033, 10.1021/jp505910w, 2014.

Duplissy, J., DeCarlo, P. F., Dommen, J., Alfarra, M. R., Metzger, A., Barmpadimos, I., Prevot, A. S. H., Weingartner, E., Tritscher, T., Gysel, M., Aiken, A. C., Jimenez, J. L., Canagaratna, M. R., Worsnop, D. R., Collins, D. R., Tomlinson, J., and Baltensperger, U.: Relating hygroscopicity and composition of organic aerosol particulate matter, Atmos. Chem. Phys., 11, 1155-1165, 10.5194/acp-11-1155-2011, 2011.

El-Sayed, M. M. H., Wang, Y. Q., and Hennigan, C. J.: Direct atmospheric evidence for the irreversible formation of aqueous secondary organic aerosol, Geophys. Res. Lett. , 42, 5577-5586, 10.1002/2015gl064556, 2015.

Ervens, B., Turpin, B. J., and Weber, R. J.: Secondary organic aerosol formation in cloud droplets and aqueous particles (aqSOA): a review of laboratory, field and model studies, Atmos. Chem.

603 Phys., 11, 11069-11102, 10.5194/acp-11-11069-2011, 2011.
604 Fountoukis, C., and Nenes, A.: ISORROPIA II: a computationally efficient thermodynamic
605 equilibrium model for K+-Ca2+-Mg2+-Nh(4)(+)-Na+-SO42--NO3--Cl--H2O aerosols, Atmos.
606 Chem. Phys., 7, 4639-4659, DOI 10.5194/acp-7-4639-2007, 2007.
607 Galloway, M. M., Chhabra, P. S., Chan, A. W. H., Surratt, J. D., Flagan, R. C., Seinfeld, J. H., and
608 Keutsch, F. N.: Glyoxal uptake on ammonium sulphate seed aerosol: reaction products and
609 reversibility of uptake under dark and irradiated conditions, Atmos. Chem. Phys. , 9, 3331-3345,
610 10.5194/acp-9-3331-2009, 2009.
611 Gkatzelis, G. I., Papanastasiou, D. K., Karydis, V. A., Hohaus, T., Liu, Y., Schmitt, S. H., Schlag, P.,
612 Fuchs, H., Novelli, A., Chen, Q., Cheng, X., Broch, S., Dong, H., Holland, F., Li, X., Liu, Y. H., Ma, X. F.,
613 Reimer, D., Rohrer, F., Shao, M., Tan, Z., Taraborrelli, D., Tillmann, R., Wang, H. C., Wang, Y., Wu, Y.
614 S., Wu, Z. J., Zeng, L. M., Zheng, J., Hu, M., Lu, K. D., Hofzumahaus, A., Zhang, Y. H., Wahner, A.,
615 and Kiendler-Scharr, A.: Uptake of Water-soluble Gas-phase Oxidation Products Drives Organic
616 Particulate Pollution in Beijing, Geophys. Res. Lett., 48, ARTN e2020GL091351

617 10.1029/2020GL091351, 2021.
618 Gunthe, S. S., Rose, D., Su, H., Garland, R. M., Achtert, P., Nowak, A., Wiedensohler, A., Kuwata, M.,
619 Takegawa, N., Kondo, Y., Hu, M., Shao, M., Zhu, T., Andreae, M. O., and Pöschl, U.: Cloud
620 condensation nuclei (CCN) from fresh and aged air pollution in the megacity region of Beijing,
621 Atmos. Chem. Phys., 11, 11023-11039, 10.5194/acp-11-11023-2011, 2011.
622 Guo, H., Xu, L., Bougiatioti, A., Cerully, K. M., Capps, S. L., Hite Jr, J. R., Carlton, A. G., Lee, S. H.,
623 Bergin, M. H., Ng, N. L., Nenes, A., and Weber, R. J.: Fine-particle water and pH in the southeastern
624 United States, Atmos. Chem. Phys., 15, 5211-5228, 10.5194/acp-15-5211-2015, 2015.
625 Gysel, M., Crosier, J., Topping, D. O., Whitehead, J. D., Bower, K. N., Cubison, M. J., Williams, P. I.,
626 Flynn, M. J., McFiggans, G. B., and Coe, H.: Closure study between chemical composition and
627 hygroscopic growth of aerosol particles during TORCH2, Atmos Chem Phys, 7, 6131-6144, 2007.
628 Herrmann, H., Schaefer, T., Tilgner, A., Styler, S. A., Weller, C., Teich, M., and Otto, T.: Tropospheric
629 Aqueous-Phase Chemistry: Kinetics, Mechanisms, and Its Coupling to a Changing Gas Phase,
630 Chem. Rev., 115, 4259-4334, 10.1021/cr500447k, 2015.
631 Hodas, N., Sullivan, A. P., Skog, K., Keutsch, F. N., Collett, J. L., Decesari, S., Facchini, M. C., Carlton,
632 A. G., Laaksonen, A., and Turpin, B. J.: Aerosol Liquid Water Driven by Anthropogenic Nitrate:
633 Implications for Lifetimes of Water-Soluble Organic Gases and Potential for Secondary Organic
634 Aerosol Formation, Environ. Sci. Technol. , 48, 11127-11136, 2014.
635 Hodas, N., Zuend, A., Mui, W., Flagan, R. C., and Seinfeld, J. H.: Influence of particle-phase state
636 on the hygroscopic behavior of mixed organic-inorganic aerosols, Atmos. Chem. Phys. , 15, 5027-
637 5045, 10.5194/acp-15-5027-2015, 2015.
638 Hu, S. Y., Zhao, G., Tan, T. Y., Li, C. C., Zong, T. M., Xu, N., Zhu, W. F., and Hu, M.: Current challenges
639 of improving visibility due to increasing nitrate fraction in PM2.5 during the haze days in Beijing,
640 China, Environ. Pollut., 290, 2021.
641 Iinuma, Y., Muller, C., Berndt, T., Boge, O., Claeys, M., and Herrmann, H.: Evidence for the existence
642 of organosulfates from beta-pinene ozonolysis in ambient secondary organic aerosol, Environ. Sci.
643 Technol., 41, 6678-6683, 10.1021/es070938t, 2007.
644 Jia, L., Xu, Y., and Duan, M.: Explosive formation of secondary organic aerosol due to aerosol-fog

interactions, Sci. Total Environ., 866, 161338, https://doi.org/10.1016/j.scitotenv.2022.161338, 2023.
Jin, X., Wang, Y., Li, Z., Zhang, F., Xu, W., Sun, Y., Fan, X., Chen, G., Wu, H., Ren, J., Wang, Q., and Cribb, M.: Significant contribution of organics to aerosol liquid water content in winter in Beijing, China, Atmos. Chem. Phys., 20, 901-914, 10.5194/acp-20-901-2020, 2020.
Knopf, D. A., and Alpert, P. A.: Atmospheric ice nucleation, Nat Rev Phys, 5, 203-217, 10.1038/s42254-023-00570-7, 2023.
Koop, T., Bookhold, J., Shiraiwa, M., and Poschl, U.: Glass transition and phase state of organic compounds: dependency on molecular properties and implications for secondary organic aerosols in the atmosphere, Phys. Chem. Chem. Phys., 13, 19238-19255, 10.1039/c1cp22617g, 2011.
Kuang, Y., He, Y., Xu, W., Zhao, P., Cheng, Y., Zhao, G., Tao, J., Ma, N., Su, H., Zhang, Y., Sun, J., Cheng, P., Yang, W., Zhang, S., Wu, C., Sun, Y., and Zhao, C.: Distinct diurnal variation in organic aerosol hygroscopicity and its relationship with oxygenated organic aerosol, Atmos. Chem. Phys., 20, 865-880, 10.5194/acp-20-865-2020, 2020.
Lei, L., Zhou, W., Chen, C., He, Y., Li, Z. J., Sun, J. X., Tang, X., Fu, P. Q., Wang, Z. F., and Sun, Y. L.: Long-term characterization of aerosol chemistry in cold season from 2013 to 2020 in Beijing, China, Environ. Pollut., 268, 2021.
Lelieveld, J., Evans, J. S., Fnais, M., Giannadaki, D., and Pozzer, A.: The contribution of outdoor air pollution sources to premature mortality on a global scale, Nature, 525, 367-371, 10.1038/nature15371, 2015.
Li, X. X., Song, S. J., Zhou, W., Hao, J. M., Worsnop, D. R., and Jiang, J. K.: Interactions between aerosol organic components and liquid water content during haze episodes in Beijing, Atmos. Chem. Phys., 19, 12163-12174, 2019.
Li, Y., and Shiraiwa, M.: Timescales of secondary organic aerosols to reach equilibrium at various temperatures and relative humidities, Atmos. Chem. Phys., 19, 5959-5971, 10.5194/acp-19-5959-2019, 2019.
Li, Y. J., Sun, Y., Zhang, Q., Li, X., Li, M., Zhou, Z., and Chan, C. K.: Real-time chemical characterization of atmospheric particulate matter in China: A review, Atmos. Environ., 158, 270-304, https://doi.org/10.1016/j.atmosenv.2017.02.027, 2017.
Li, Z., Smith, K. A., and Cappa, C. D.: Influence of relative humidity on the heterogeneous oxidation of secondary organic aerosol, Atmos. Chem. Phys., 18, 14585-14608, 10.5194/acp-18-14585-2018, 2018.
Lim, Y. B., Tan, Y., Perri, M. J., Seitzinger, S. P., and Turpin, B. J.: Aqueous chemistry and its role in secondary organic aerosol (SOA) formation, Atmos. Chem. Phys., 10, 10521-10539, 10.5194/acp-10-10521-2010, 2010.
Lim, Y. B., Tan, Y., and Turpin, B. J.: Chemical insights, explicit chemistry, and yields of secondary organic aerosol from OH radical oxidation of methylglyoxal and glyoxal in the aqueous phase, Atmos. Chem. Phys. , 13, 8651-8667, 10.5194/acp-13-8651-2013, 2013.
Liu, P., Song, M., Zhao, T., Gunthe, S. S., Ham, S., He, Y., Qin, Y. M., Gong, Z., Amorim, J. C., Bertram, A. K., and Martin, S. T.: Resolving the mechanisms of hygroscopic growth and cloud condensation nuclei activity for organic particulate matter, Nat. Commun., 9, 4076, 10.1038/s41467-018-06622-2, 2018.
Liu, T., Clegg, S. L., and Abbatt, J. P. D.: Fast oxidation of sulfur dioxide by hydrogen peroxide in

deliquesced aerosol particles, Proc. Natl. Acad. Sci. U.S.A. , 117, 1354-1359, doi:10.1073/pnas.1916401117, 2020.
Liu, Y., Wu, Z., Wang, Y., Xiao, Y., Gu, F., Zheng, J., Tan, T., Shang, D., Wu, Y., Zeng, L., Hu, M., Bateman, A. P., and Martin, S. T.: Submicrometer Particles Are in the Liquid State during Heavy Haze Episodes in the Urban Atmosphere of Beijing, China, Environ. Sci. Technol. Lett. , 4, 427-432, 10.1021/acs.estlett.7b00352, 2017.
Liu, Y., Wu, Z., Huang, X., Shen, H., Bai, Y., Qiao, K., Meng, X., Hu, W., Tang, M., and He, L.: Aerosol Phase State and Its Link to Chemical Composition and Liquid Water Content in a Subtropical Coastal Megacity, Environ. Sci. Technol. , 53, 5027-5033, 10.1021/acs.est.9b01196, 2019.
Liu, Y. C., Meng, X. X., Wu, Z. J., Huang, D. D., Wang, H. L., Chen, J., Chen, J. C., Zong, T. M., Fang, X., Tan, T. Y., Zhao, G., Chen, S. Y., Zeng, L. W., Guo, S., Huang, X. F., He, L. Y., Zeng, L. M., and Hu, M.: The particle phase state during the biomass burning events, Sci. Total Environ., 792, ARTN 148035
10.1016/j.scitotenv.2021.148035, 2021.
Ma, W., Zheng, F. X., Zhang, Y. S., Chen, X., Zhan, J. L., Hua, C. J., Song, B. Y., Wang, Z. C., Xie, J. L., Yan, C., Kulmala, M., and Liu, Y. C.: Weakened Gas-to-Particle Partitioning of Oxygenated Organic Molecules in Liquified Aerosol Particles, Environ. Sci. Technol. Lett., 10.1021/acs.estlett.2c00556, 2022.
Marshall, F. H., Berkemeier, T., Shiraiwa, M., Nandy, L., Ohm, P. B., Dutcher, C. S., and Reid, J. P.: Influence of particle viscosity on mass transfer and heterogeneous ozonolysis kinetics in aqueous-sucrose-maleic acid aerosol, Phys. Chem. Chem. Phys., 20, 15560-15573, 2018.
Matthew, B. M., Middlebrook, A. M., and Onasch, T. B.: Collection efficiencies in an Aerodyne Aerosol Mass Spectrometer as a function of particle phase for laboratory generated aerosols, Aerosol Sci. Technol., 42, 884-898, 10.1080/02786820802356797, 2008.
Meng, X. X. Y., Wu, Z. J., Guo, S., Wang, H., Liu, K. F., Zong, T. M., Liu, Y. C., Zhang, W. B., Zhang, Z., Chen, S. Y., Zeng, L. M., Hallquist, M., Shuai, S. J., and Hu, M.: Humidity-Dependent Phase State of Gasoline Vehicle Emission-Related Aerosols, Environ. Sci. Technol. , 55, 832-841, 2021.
Mikhailov, E., Vlasenko, S., Martin, S. T., Koop, T., and Poschl, U.: Amorphous and crystalline aerosol particles interacting with water vapor: conceptual framework and experimental evidence for restructuring, phase transitions and kinetic limitations, Atmos. Chem. Phys., 9, 9491-9522, 2009.
Mu, Q., Shiraiwa, M., Octaviani, M., Ma, N., Ding, A. J., Su, H., Lammel, G., Poschl, U., and Cheng, Y. F.: Temperature effect on phase state and reactivity controls atmospheric multiphase chemistry and transport of PAHs, Sci. Adv., 4, 2018.
Murray, B. J., Wilson, T. W., Dobbie, S., Cui, Z. Q., Al-Jumur, S. M. R. K., Mohler, O., Schnaiter, M., Wagner, R., Benz, S., Niemand, M., Saathoff, H., Ebert, V., Wagner, S., and Karcher, B.: Heterogeneous nucleation of ice particles on glassy aerosols under cirrus conditions, Nat. Geosci., 3, 233-237, 2010.
Ng, N. L., Canagaratna, M. R., Zhang, Q., Jimenez, J. L., Tian, J., Ulbrich, I. M., Kroll, J. H., Docherty, K. S., Chhabra, P. S., Bahreini, R., Murphy, S. M., Seinfeld, J. H., Hildebrandt, L., Donahue, N. M., DeCarlo, P. F., Lanz, V. A., Prevot, A. S. H., Dinar, E., Rudich, Y., and Worsnop, D. R.: Organic aerosol components observed in Northern Hemispheric datasets from Aerosol Mass Spectrometry, Atmos. Chem. Phys., 10, 4625-4641, 10.5194/acp-10-4625-2010, 2010.

730 Ng, N. L., Herndon, S. C., Trimborn, A., Canagaratna, M. R., Croteau, P. L., Onasch, T. B., Sueper, D.,
731 Worsnop, D. R., Zhang, Q., Sun, Y. L., and Jayne, J. T.: An Aerosol Chemical Speciation Monitor
732 (ACSM) for Routine Monitoring of the Composition and Mass Concentrations of Ambient Aerosol,
733 Aerosol Sci. Technol., 45, 780-794, Pii 934555189

734 10.1080/02786826.2011.560211, 2011.
735 Nguyen, T. K. V., Zhang, Q., Jimenez, J. L., Pike, M., and Carlton, A. G.: Liquid Water: Ubiquitous
736 Contributor to Aerosol Mass, Environ. Sci. Technol. Lett. , 3, 257-263, 2016.
737 Pajunoja, A., Hu, W. W., Leong, Y. J., Taylor, N. F., Miettinen, P., Palm, B. B., Mikkonen, S., Collins,
738 D. R., Jimenez, J. L., and Virtanen, A.: Phase state of ambient aerosol linked with water uptake and
739 chemical aging in the southeastern US, Atmos. Chem. Phys., 16, 11163-11176, 2016.
740 Peckhaus, A., Grass, S., Treuel, L., and Zellner, R.: Deliquescence and Efflorescence Behavior of
741 Ternary Inorganic/Organic/Water Aerosol Particles, J. Phys. Chem. A, 116, 6199-6210,
742 10.1021/jp211522t, 2012.
743 Peng, C., Chen, L. X. D., and Tang, M. J.: A database for deliquescence and efflorescence relative
744 humidities of compounds with atmospheric relevance, Fund Res-China, 2, 578-587,
745 10.1016/j.fmre.2021.11.021, 2022.
746 Petters, M. D., and Kreidenweis, S. M.: A single parameter representation of hygroscopic growth
747 and cloud condensation nucleus activity, Atmos. Chem. Phys., 7, 1961-1971, 2007.
748 Petters, S. S., Kreidenweis, S. M., Grieshop, A. P., Ziemann, P. J., and Petters, M. D.: Temperature-
749 and Humidity-Dependent Phase States of Secondary Organic Aerosols, Geophys Res Lett, 46,
750 1005-1013, https://doi.org/10.1029/2018GL080563, 2019.
751 Pöschl, U.: Atmospheric Aerosols: Composition, Transformation, Climate and Health Effects,
752 Angewandte Chemie International Edition, 44, 7520-7540,
753 https://doi.org/10.1002/anie.200501122, 2005.
754 Ravishankara, A. R.: Heterogeneous and multiphase chemistry in the troposphere, Science, 276,
755 1058-1065, 1997.
756 Rothfuss, N. E., and Petters, M. D.: Influence of Functional Groups on the Viscosity of Organic
757 Aerosol, Environmental Science & Technology, 51, 271-279, 10.1021/acs.est.6b04478, 2017.
758 Saukko, E., Lambe, A. T., Massoli, P., Koop, T., Wright, J. P., Croasdale, D. R., Pedernera, D. A.,
759 Onasch, T. B., Laaksonen, A., Davidovits, P., Worsnop, D. R., and Virtanen, A.: Humidity-dependent
760 phase state of SOA particles from biogenic and anthropogenic precursors, Atmos Chem Phys, 12,
761 7517-7529, 2012.
762 Seinfeld, J. H., Bretherton, C., Carslaw, K. S., Coe, H., DeMott, P. J., Dunlea, E. J., Feingold, G., Ghan,
763 S., Guenther, A. B., Kahn, R., Kraucunas, I., Kreidenweis, S. M., Molina, M. J., Nenes, A., Penner, J. E.,
764 Prather, K. A., Ramanathan, V., Ramaswamy, V., Rasch, P. J., Ravishankara, A. R., Rosenfeld, D.,

765 Stephens, G., and Wood, R.: Improving our fundamental understanding of the role of aerosol–

766 cloud interactions in the climate system, Proc. Natl. Acad. Sci. U. S. A., 113, 5781-5790,
767 doi:10.1073/pnas.1514043113, 2016.
768 Seinfeld, J. H., and Pendis, S. N.: Atmospheric Chemistry and Physics: From Air Pollution to Climate
769 Change, Wiley, 2006.
770 Shen, H., Chen, Z., Li, H., Qian, X., Qin, X., and Shi, W.: Gas-Particle Partitioning of Carbonyl

771 Compounds in the Ambient Atmosphere, Environmental Science & Technology, 52, 10997-11006,
772 10.1021/acs.est.8b01882, 2018.
773 Shiraiwa, M., Ammann, M., Koop, T., and Poschl, U.: Gas uptake and chemical aging of semisolid
774 organic aerosol particles, Proc. Natl. Acad. Sci. U. S. A., 108, 11003-11008,
775 10.1073/pnas.1103045108, 2011.
776 Shiraiwa, M., Zuend, A., Bertram, A. K., and Seinfeld, J. H.: Gas-particle partitioning of atmospheric
777 aerosols: interplay of physical state, non-ideal mixing and morphology, Phys. Chem. Chem. Phys.,
778 15, 11441-11453, 2013.
779 Shiraiwa, M., Li, Y., Tsimpidi, A. P., Karydis, V. A., Berkemeier, T., Pandis, S. N., Lelieveld, J., Koop, T.,
780 and Poschl, U.: Global distribution of particle phase state in atmospheric secondary organic
781 aerosols, Nature Communications, 8, 2017.
782 Song, M., Jeong, R., Kim, D., Qiu, Y., Meng, X., Wu, Z., Zuend, A., Ha, Y., Kim, C., Kim, H., Gaikwad,
783 S., Jang, K.-S., Lee, J. Y., and Ahn, J.: Comparison of Phase States of PM2.5 over Megacities, Seoul
784 and Beijing, and Their Implications on Particle Size Distribution, Environ. Sci. Technol. ,
785 10.1021/acs.est.2c06377, 2022.
786 Song, M. J., Marcolli, C., Krieger, U. K., Lienhard, D. M., and Peter, T.: Morphologies of mixed
787 organic/inorganic/aqueous aerosol droplets, Faraday Discuss., 165, 289-316, 2013.
788 Sun, Y. L., Wang, Z. F., Fu, P. Q., Yang, T., Jiang, Q., Dong, H. B., Li, J., and Jia, J. J.: Aerosol
789 composition, sources and processes during wintertime in Beijing, China, Atmos. Chem. Phys., 13,
790 4577-4592, 10.5194/acp-13-4577-2013, 2013.
791 Sun, Y. L., Du, W., Wang, Q. Q., Zhang, Q., Chen, C., Chen, Y., Chen, Z. Y., Fu, P. Q., Wang, Z. F.,
792 Gao, Z. Q., and R., W. D.: Real-Time Characterization of Aerosol Particle Composition above the
793 Urban Canopy in Beijing: Insights into the Interactions between the Atmospheric Boundary Layer
794 and Aerosol Chemistry, Environ. Sci. Technol. , 2015 v.49 no.19, pp. 11340-11347,
795 10.1021/acs.est.5b02373, 2015.
796 Surratt, J. D., Kroll, J. H., Kleindienst, T. E., Edney, E. O., Claeys, M., Sorooshian, A., Ng, N. L.,
797 Offenberg, J. H., Lewandowski, M., Jaoui, M., Flagan, R. C., and Seinfeld, J. H.: Evidence for
798 organosulfates in secondary organic aerosol, Environ. Sci. Technol., 41, 517-527,
799 10.1021/es062081q, 2007.
800 Tang, M. J., Cox, R. A., and Kalberer, M.: Compilation and evaluation of gas phase diffusion
801 coefficients of reactive trace gases in the atmosphere: volume 1. Inorganic compounds, Atmos.
802 Chem. Phys., 14, 9233-9247, 10.5194/acp-14-9233-2014, 2014.
803 Tillmann, R., Hallquist, M., Jonsson, Å. M., Kiendler-Scharr, A., Saathoff, H., Iinuma, Y., and Mentel,
804 T. F.: Influence of relative humidity and temperature on the production of pinonaldehyde and OH
805 radicals from the ozonolysis of α-pinene, Atmos. Chem. Phys., 10, 7057-7072, 10.5194/acp-
806 10-7057-2010, 2010.
807 Ushijima, S. B., Huynh, E., Davis, R. D., and Tolbert, M. A.: Seeded Crystal Growth of Internally Mixed
808 Organic-Inorganic Aerosols: Impact of Organic Phase State, J. Phys. Chem. A, 125, 8668-8679,
809 10.1021/acs.jpca.1c04471, 2021.
810 Wang, H., Chen, X., Lu, K., Tan, Z., Ma, X., Wu, Z., Li, X., Liu, Y., Shang, D., Wu, Y., Zeng, L., Hu, M.,
811 Schmitt, S., Kiendler-Scharr, A., Wahner, A., and Zhang, Y.: Wintertime N2O5 uptake coefficients
812 over the North China Plain, Sci. Bull., 65, 765-774, https://doi.org/10.1016/j.scib.2020.02.006,
813 2020a.

Wang, J. F., Ye, J. H., Zhang, Q., Zhao, J., Wu, Y. Z., Li, J. Y., Liu, D. T., Li, W. J., Zhang, Y. G., Wu, C., Xie, C. H., Qin, Y. M., Lei, Y. L., Huang, X. P., Guo, J. P., Liu, P. F., Fu, P. Q., Li, Y. J., Lee, H. C., Choi, H., Zhang, J., Liao, H., Chen, M. D., Sun, Y. L., Ge, X. L., Martin, S. T., and Jacob, D. J.: Aqueous production of secondary organic aerosol from fossil-fuel emissions in winter Beijing haze, Proc. Natl. Acad. Sci. U.S.A. , 118, 2021a.

Wang, Y., Chen, Y., Wu, Z. J., Shang, D. J., Bian, Y. X., Du, Z. F., Schmitt, S. H., Su, R., Gkatzelis, G. I., Schlag, P., Hohaus, T., Voliotis, A., Lu, K. D., Zen, L. M., Zhao, C. S., Alfarra, M. R., McFiggans, G., Wiedensohler, A., Kiendler-Scharr, A., Zhang, Y. H., and Hu, M.: Mutual promotion between aerosol particle liquid water and particulate nitrate enhancement leads to severe nitrate-dominated particulate matter pollution and low visibility, Atmos. Chem. Phys., 20, 2161-2175, 2020b.

Wang, Y., Hu, M., Wang, Y.-C., Li, X., Fang, X., Tang, R., Lu, S., Wu, Y., Guo, S., Wu, Z., Hallquist, M., and Yu, J. Z.: Comparative Study of Particulate Organosulfates in Contrasting Atmospheric Environments: Field Evidence for the Significant Influence of Anthropogenic Sulfate and NOx, Environ. Sci. Technol. Lett., 7, 787-794, 10.1021/acs.estlett.0c00550, 2020c.

Wang, Y. Y., Li, Z. Q., Wang, Q. Y., Jin, X. A., Yan, P., Cribb, M., Li, Y. A., Yuan, C., Wu, H., Wu, T., Ren, R. M., and Cai, Z. X.: Enhancement of secondary aerosol formation by reduced anthropogenic emissions during Spring Festival 2019 and enlightenment for regional PM2.5 control in Beijing, Atmos. Chem. Phys., 21, 915-926, 2021b.

Williams, B. J., Goldstein, A. H., Kreisberg, N. M., and Hering, S. V.: In situ measurements of gas/particle-phase transitions for atmospheric semivolatile organic compounds, Proceedings of the National Academy of Sciences, 107, 6676-6681, doi:10.1073/pnas.0911858107, 2010.

Wu, Z. J., Zheng, J., Shang, D. J., Du, Z. F., Wu, Y. S., Zeng, L. M., Wiedensohler, A., and Hu, M.: Particle hygroscopicity and its link to chemical composition in the urban atmosphere of Beijing, China, during summertime, Atmos. Chem. Phys., 16, 1123-1138, 10.5194/acp-16-1123-2016, 2016.

Wu, Z. J., Wang, Y., Tan, T. Y., Zhu, Y. S., Li, M. R., Shang, D. J., Wang, H. C., Lu, K. D., Guo, S., Zeng, L. M., and Zhang, Y. H.: Aerosol Liquid Water Driven by Anthropogenic Inorganic Salts: Implying Its Key Role in Haze Formation over the North China Plain, Environ. Sci. Technol. Lett. , 5, 160-166, 2018.

Xu, W. Q., Han, T. T., Du, W., Wang, Q. Q., Chen, C., Zhao, J., Zhang, Y. J., Li, J., Fu, P. Q., Wang, Z. F., Worsnop, D. R., and Sun, Y. L.: Effects of Aqueous-Phase and Photochemical Processing on Secondary Organic Aerosol Formation and Evolution in Beijing, China, Environ. Sci. Technol., 51, 762-770, 10.1021/acs.est.6b04498, 2017.

Zhang, Q., Jimenez, J. L., Canagaratna, M. R., Ulbrich, I. M., Ng, N. L., Worsnop, D. R., and Sun, Y.: Understanding atmospheric organic aerosols via factor analysis of aerosol mass spectrometry: a review, Anal. Bioanal. Chem., 401, 3045-3067, 10.1007/s00216-011-5355-y, 2011.

Zhang, Y., Chen, Y. Z., Lambe, A. T., Olson, N. E., Lei, Z. Y., Craig, R. L., Zhang, Z. F., Gold, A., Onasch, T. B., Jayne, J. T., Worsnop, D. R., Gaston, C. J., Thornton, J. A., Vizuete, W., Ault, A. P., and Surratt, J. D.: Effect of the Aerosol-Phase State on Secondary Organic Aerosol Formation from the Reactive Uptake of Isoprene-Derived Epoxydiols (IEPDX), Environ. Sci. Technol. Lett. , 5, 167-174, 2018.

Zhang, Y. J., Tang, L. L., Croteau, P. L., Favez, O., Sun, Y. L., Canagaratna, M. R., Wang, Z., Couvidat, F., Albinet, A., Zhang, H. L., Sciare, J., Prevot, A. S. H., Jayne, J. T., and Worsnop, D. R.: Field characterization of the PM2.5 Aerosol Chemical Speciation Monitor: insights into the composition,

sources, and processes of fine particles in eastern China, Atmos. Chem. Phys., 17, 14501-14517, 10.5194/acp-17-14501-2017, 2017.
Zhao, Z., Xu, Q., Yang, X., and Zhang, H.: Heterogeneous Ozonolysis of Endocyclic Unsaturated Organic Aerosol Proxies: Implications for Criegee Intermediate Dynamics and Later-Generation Reactions, ACS Earth Space Chem., 3, 344-356, 10.1021/acsearthspacechem.8b00177, 2019.
Zheng, B., Zhang, Q., Zhang, Y., He, K. B., Wang, K., Zheng, G. J., Duan, F. K., Ma, Y. L., and Kimoto, T.: Heterogeneous chemistry: a mechanism missing in current models to explain secondary inorganic aerosol formation during the January 2013 haze episode in North China, Atmos. Chem. Phys., 15, 2031-2049, 10.5194/acp-15-2031-2015, 2015.
Zheng, Y., Chen, Q., Cheng, X., Mohr, C., Cai, J., Huang, W., Shrivastava, M., Ye, P., Fu, P., Shi, X., Ge, Y., Liao, K., Miao, R., Qiu, X., Koenig, T. K., and Chen, S.: Precursors and Pathways Leading to Enhanced Secondary Organic Aerosol Formation during Severe Haze Episodes, Environ. Sci. Technol., 55, 15680-15693, 10.1021/acs.est.1c04255, 2021.
Zheng, Y., Miao, R. Q., Zhang, Q., Li, Y. W., Cheng, X., Liao, K. R., Koenig, T. K., Ge, Y. L., Tang, L. Z., Shang, D. J., Hu, M., Chen, S. Y., and Chen, Q.: Secondary Formation of Submicron and Supermicron Organic and Inorganic Aerosols in a Highly Polluted Urban Area, J. Geophys. Res. Atmos., 128, 10.1029/2022jd037865, 2023.

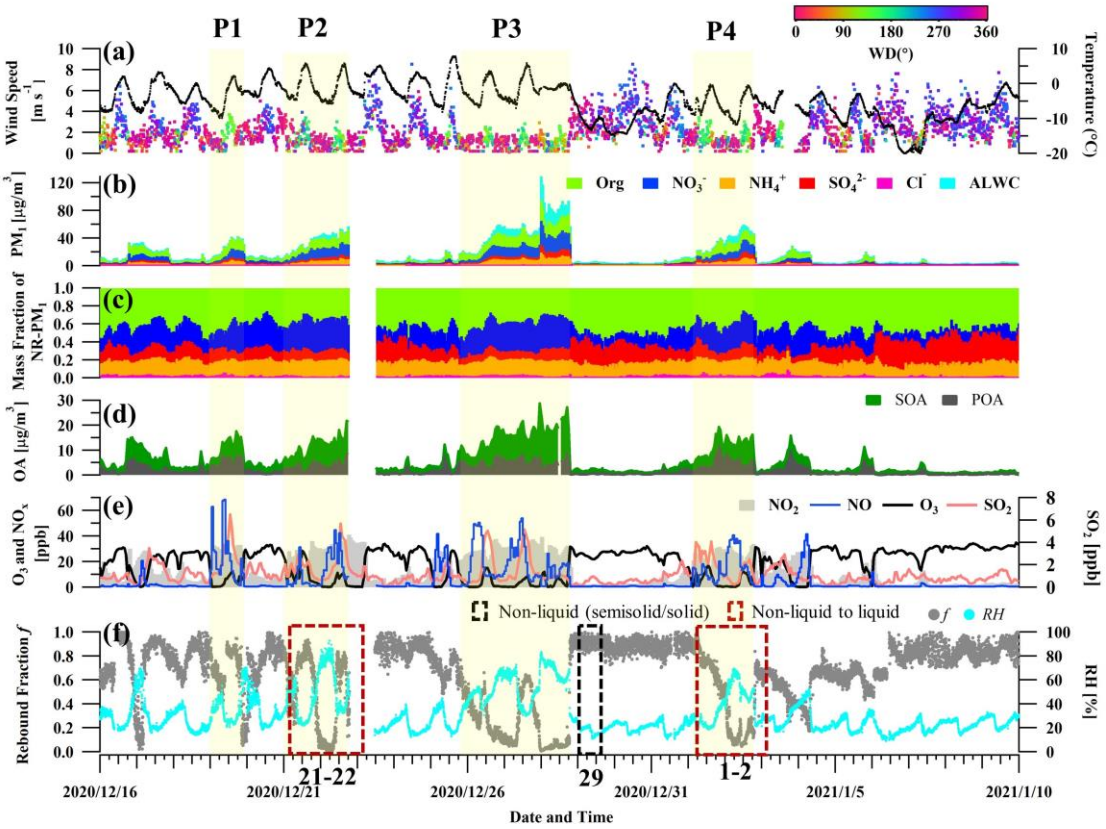

Figure 1. Time series of (a) wind speed (WS), wind direction (WD) and temperatures, (b) mass concentration of NR-PM_1 and ALW, (c) mass contribution of NR-PM_1, (d) mass concentrations of SOA and POA, (e) concentrations of gas pollutants (NO_2, NO, O_3, and SO_2), (f) rebound fraction and ambient RH during the field campaign. In panel (f), the black (red) frame with dashed line represents the non-liquid state (transition from non-liquid to liquid state) of bulk $PM_{2.5}$ droplets based on off-line viscosity measurement using poke-and-flow technique (Song et al., 2022).

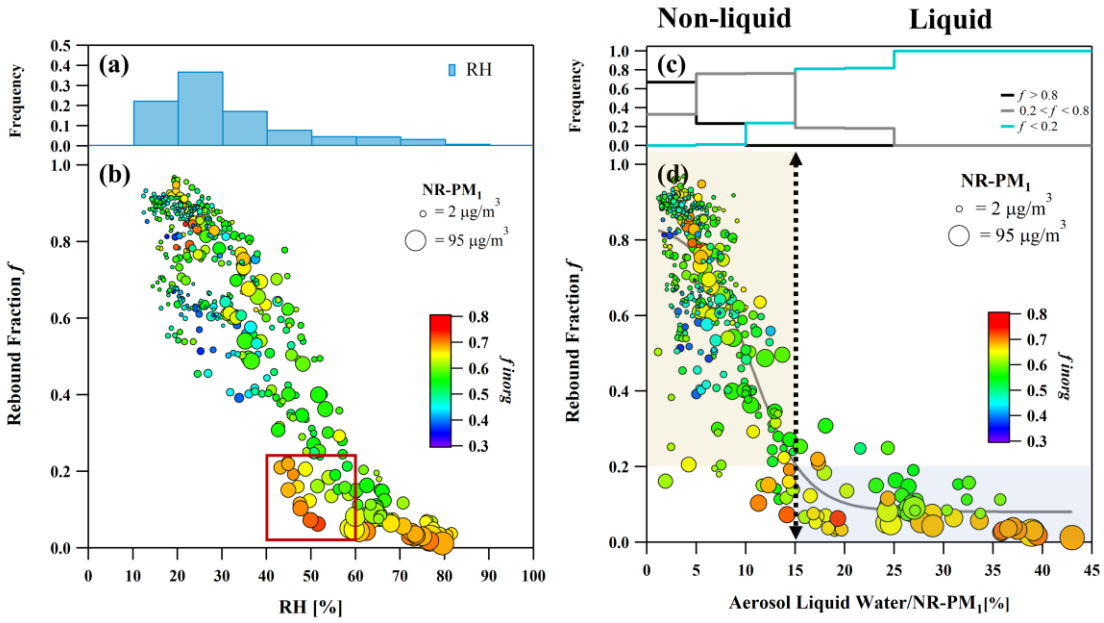

884

885 Figure 2. The frequency distribution of ambient RH in each RH bin (a) and the
886 frequency distribution of each f interval in each ALW/NR-PM_1 bin (c). Rebound
887 fraction f as a function of ambient RH (b) and ALW/NR-PM_1 (d) during the observation.
888 In panel (b) and (d), the scatter points are colored by f_{inorg} in NR-PM_1 and the point size
889 is scaled by NR-PM_1 mass concentration. The yellow and blue shadow represent the
890 non-liquid and liquid phase, respectively.

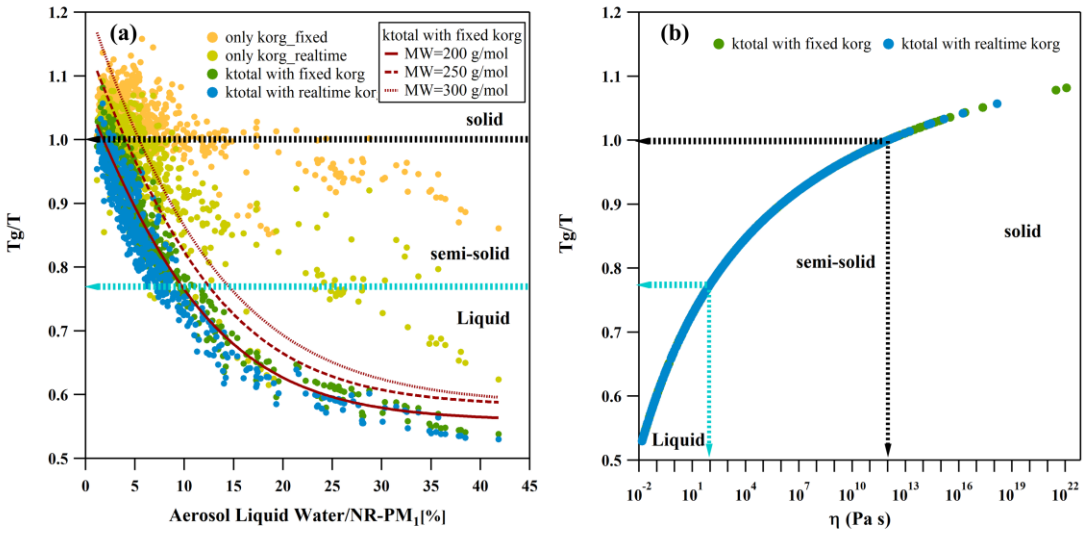

891

892 Figure 3. Characteristic relations between T_g/T and ALW/NR-PM_1 (a) and T_g/T as a
893 function of predicted viscosity η (b) of organic aerosols under ambient conditions. In
894 panel (a), the red curves, which employ sigmoid fitting, represent variations in average
895 molecular weights of OA used for T_g calculation in consideration of the total
896 hygroscopicity of the particles. The characteristics of the particle-phase state are
897 delineated by arrows and dashed lines.

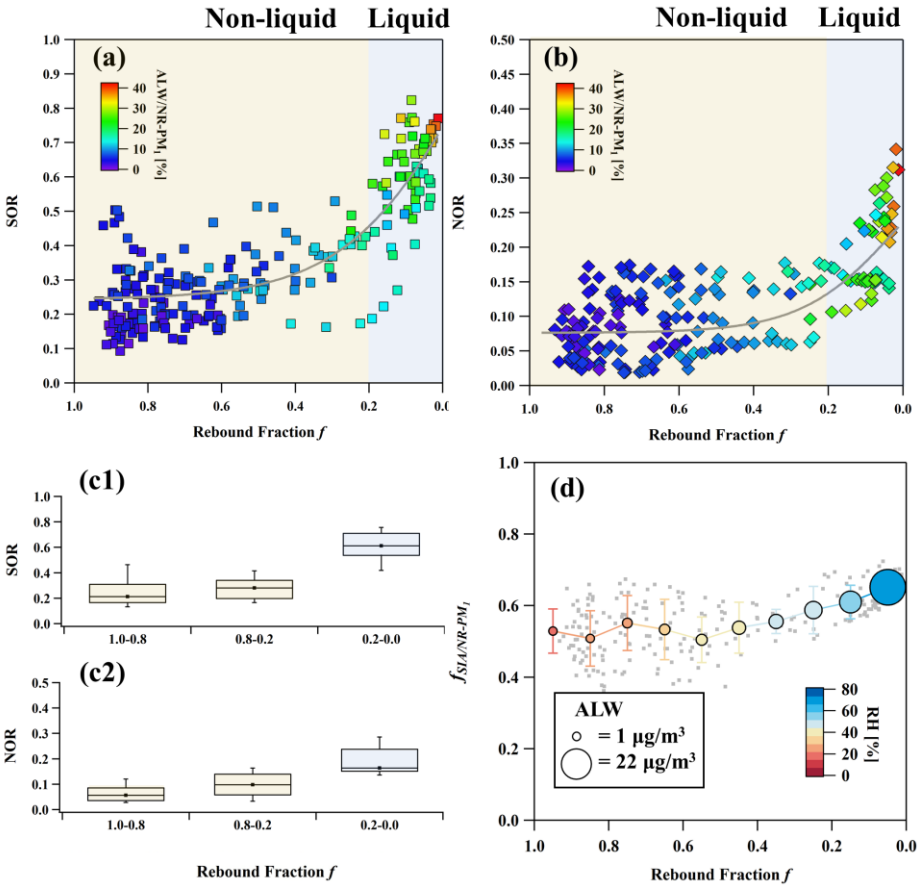

898

899 Figure 4. SOR and NOR as a function of *f* (a, b), relationship between SOR or NOR
900 and three phase transition level (c1, c2), and the mass fraction of SIA in NR-PM_1 as a
901 function of *f* during haze episodes (d). Non-liquid particles are marked by yellow
902 shadows and liquid particles are marked by blue shadows. In panel (a) and (b), the
903 scatter points are colored by ALW/NR-PM_1 and the trend lines are obtained by sigmoid
904 fitting. In panel (c1) and (c2), the box plots show 10th, 25th, median,75th and 90th
905 percentiles. In panel (d), RH is indicated by color, and ALW mass concentration is
906 indicated by the size of the circle. The error bars show one standard deviation.

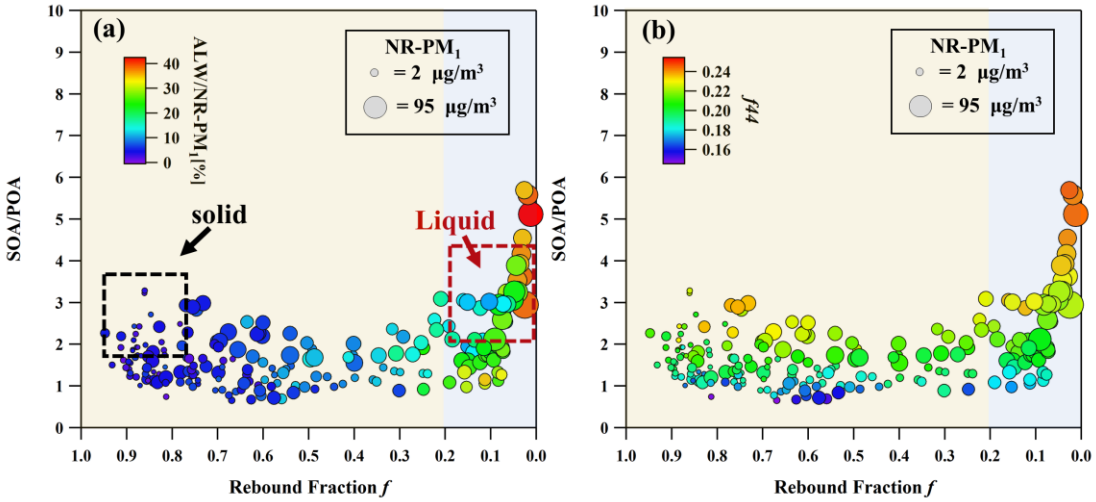

907

908 Figure 5. The relationship between SOA/POA and particle rebound fraction *f* for phase
909 transition (a) and oxidation degree (b) during haze episodes. Non-liquid particles are
910 marked by yellow shadows and liquid particles are marked by blue shadows. The circles
911 are colored by ALW/NR-PM_1 and f_{44} to represent water uptake capacity and particle
912 oxidation degree in panel (a) and panel (b), respectively. The sizes of the circles are
913 scaled to NR-PM_1 mass concentrations. The black (red) frame with dashed line
914 represent the off-line viscosity measurement results using poke-and-flow technique
915 corresponding to Figure 1.

916

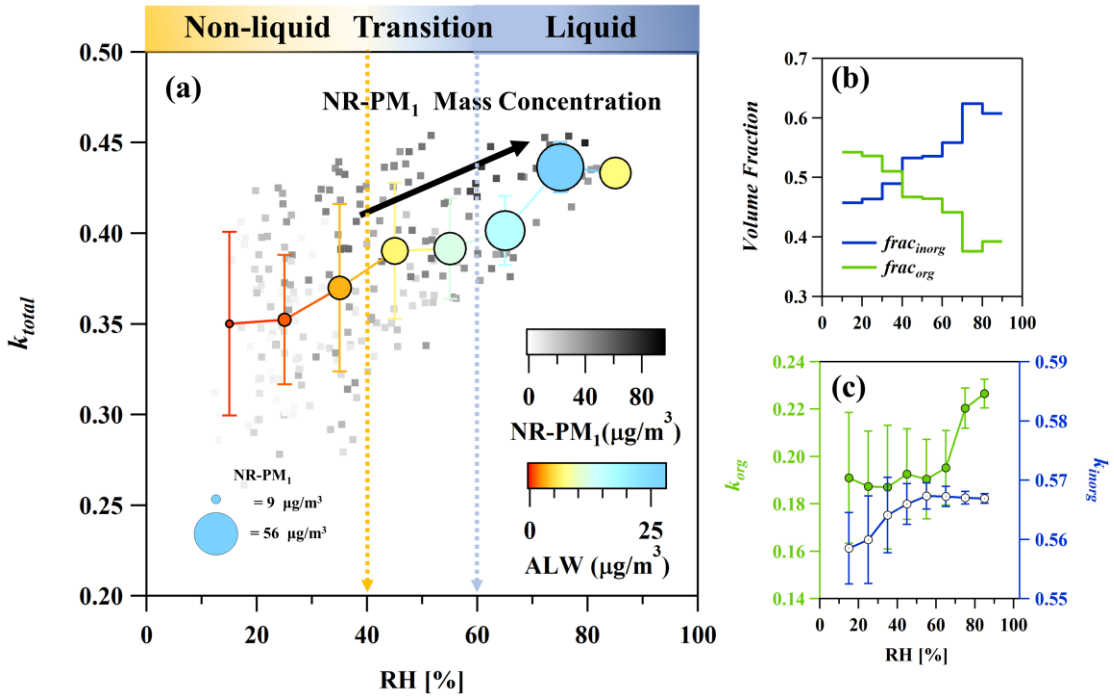

Figure 6. The overall hygroscopicity of particles (a), average volume fraction (b) and hygroscopicity (c) of inorganics and organics as a function of RH during haze episodes. k_{total} was calculated using real-time k_{org}. Particles in different phase state condition, including non-liquid, phase transition from non-liquid to liquid, and liquid, are visually distinguished through a gradual color change from yellow to blue, which correlates with RH. In panel (a), the scatter points are colored by NR-PM_1 mass concentrations and averaged in each RH bin. Averaged ALW and NR-PM_1 mass concentrations are indicated by color and the size of the circle, respectively. The error bars show one standard deviation.